GEOPHYSICAL RESEARCH LETTERS, VOL. 27, NO. 15, PAGES 2349-2352, AUGUST 1, 2000

Solar Cycle Dependence of the Geomagnetically Trapped Anomalous Cosmic Rays

R. S. Selesnick

The Aerospace Corporation, Los Angeles

A. C. Cummings, R. A. Leske, R. A. Mewaldt, E. C. Stone

California Institute of Technology, Pasadena

J. R. Cummings

Washington University, St. Louis

Abstract. Solar cycle variations in the intensity of geomagnetically trapped anomalous cosmic ray (ACR) oxygen are demonstrated by ~7 years of data from the SAMPEX satellite. They correspond to similar variations in the interplanetary ACR source. Trapped particle losses during the approach to solar maximum are not associated with geomagnetic activity and may be consistent with atmospheric energy degradation. The average trapped particle pitch angle distribution and energy spectra support this interpretation in which both source and loss rates are proportional to atmospheric density.

Introduction

The trapping of anomalous cosmic rays (ACR) in the Earth's magnetosphere was predicted soon after their discovery [*Blake and Friesen*, 1976]. The first experimental evidence for trapped ACR came from the Cosmos satellites [*Grigorov et al.*, 1991]. Confirmation of this discovery, with detailed measurements of the trapped particles' location, elemental composition, energy spectrum, and pitch angle distribution, was made with data from the low altitude SAMPEX satellite [*Cummings et al.*, 1993; *Selesnick et al.*, 1995a,b; *Looper et al.*, 1996; *Selesnick et al.*, 1997; *Mazur et al.*, 1999] and more recently from the MIDORI satellite [*Miyasaka et al.*, 1999]. We now have ~7 years of data from SAMPEX including the minimum phase of the solar cycle, when the interplanetary ACR are most abundant, and the recent approach to solar maximum. We therefore have the opportunity to investigate the response of the trapped ACR to solar cycle variations in the interplanetary source. The continuing acquisition of data also improves the statistical accuracy of the derived particle distributions. In this letter we describe the observations of the trapped ACR oxygen, the most abundant trapped ACR element, made by the MAST instrument on SAMPEX [*Cook et al.*, 1993], and discuss implications for the trapping process, particle lifetimes, and loss mechanisms.

Observations

Our analysis technique was described in detail previously [*Selesnick et al.*, 1995a] and we give only brief summary here. The data are collected at a rate of a few ions per day. Therefore it is necessary to collect them over an extended period to obtain information on the average properties of the particle distribution function. To facilitate this we assume that the intensity is a separable function $j_1(E, \alpha_1, L, t) = U(E, L)V(\alpha_1)W(t)$ of the kinetic energy per nucleon E, pitch angle α_1, L shell, and time t. The three functions U, V, and W are determined by an iterative procedure taking into account the MAST geometry and the varying satellite position and orientation. The subscript 1 indicates that the intensity and pitch angle are evaluated at a common dipole-equivalent radius $R = 1.3$ that is near the maximum altitude reached by SAMPEX in its orbits over the South Atlantic region where the data were collected. The local pitch angles α are readily converted to α_1, thus providing a reference location for compiling the pitch angle distribution.

Time dependence

The function $W(t)$ that contains the time dependence of the trapped ACR oxygen intensity is shown with 52-day time resolution in Figure 1. It is normalized to represent the intensity at $E = 17$ MeV/nucleon and $L = 2$. The interplanetary ACR oxygen measurements in the figure from SAMPEX (8 to 27 MeV/nucleon) and ACE (7.1 to 29.4 MeV/nucleon) have been scaled to also represent the intensity at 17 MeV/nucleon using a nominal ACR energy spectrum. Also shown are the 27-day average Climax neutron monitor rate [*http://odysseus.uchicago.edu/NeutronMonitor*] scaled to match the time variability of the interplanetary ACR, the ratio of the trapped to interplanetary ACR intensities below, and the 27-day average solar 10.7 cm radio flux ($F_{10.7}$) [*ftp://ftp.ngdc.noaa.gov/STP/SOLAR_DATA*] below that.

The solar cycle dependencies of both the trapped and interplanetary ACR are clearly evident in Figure 1. The intensities generally increase during the approach to solar minimum from 1992 to 1995, are relatively steady during the solar minimum period from 1995 to 1997, and decrease during the subsequent approach to solar maximum. These variations are also mirrored in the scaled neutron monitor rate, which generally reflects the solar modulation of higher energy cosmic rays, although the ACR recovered more quickly than the neutron monitor rate prior to solar minimum [*Mewaldt et al.*, 1993]. The cosmic ray intensities

Paper number 2000GL000049.
0094-8276/00/2000GL000049$05.00

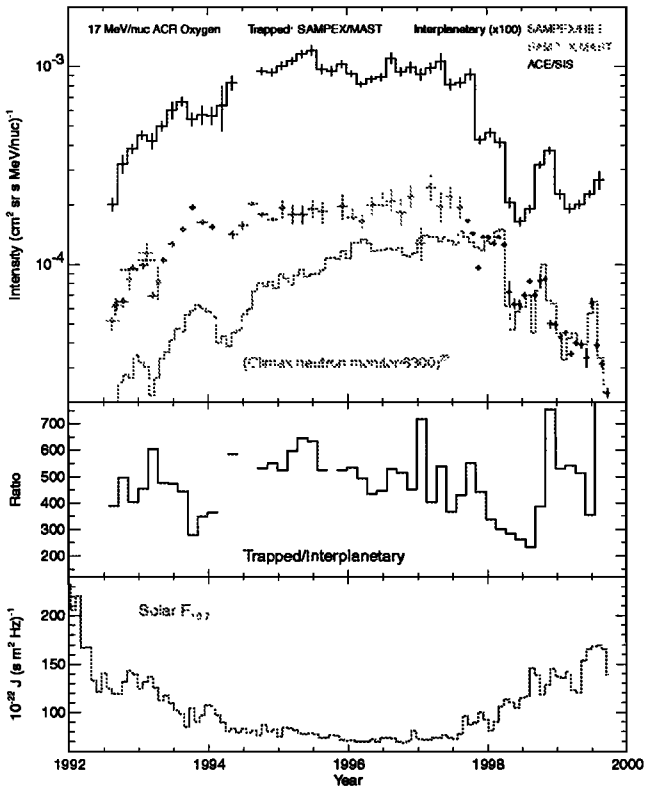

Figure 1. Trapped ACR oxygen intensity at 17 MeV/nucleon and $L = 2$ versus time with 52-day averages. Also shown are the corresponding interplanetary ACR intensity (×100), 27-day averaged scaled neutron monitor rate, the ratio of trapped to interplanetary intensities, and the 27-day averaged solar 10.7 cm radio flux.

are inversely related to $F_{10.7}$ which directly reflects the solar activity cycle.

Although the solar cycle dependence described above is clear in both ACR components, the variations are not smooth. The period of generally decreasing intensity following late 1997 shows particularly large and rapid fluctuations. Observations from this period are shown with an expanded time scale in Figure 2. The upper section has the same format as in Figure 1 except that the trapped and interplanetary ACR intensities are shown with 13.5-day resolution. (Interplanetary ACR measurements are not available during periods of significant solar particle intensities.) Daily averages of the geomagnetic D_{st} index are shown below and daily $F_{10.7}$ below that. Large negative values of D_{st} are indicative of geomagnetic storms. During this period the neutron monitor rate correlates well with the interplanetary ACR intensity and reflects the solar modulation with better time resolution, although it also shows some correlation with the D_{st} index on short time scales. The trapped ACR intensity generally follows the same trend as the interplanetary ACR and neutron monitor, but there are some differences. For example, the rapid drop (Forbush decrease) in the interplanetary ACR and neutron monitor rate near 1998.25 appears as a more gradual and earlier decrease in the trapped ACR intensity. The smaller interplanetary ACR drop near 1998.85 appears later, near 1999.0, in the trapped ACR. The ratio of the trapped to ACR intensity varied substantially throughout the period of Figure 1 with low values of ~200 and high values of ~700 (the magnitude of this ratio is dependent on the spatial location of the trapped ACR measurement and on energy, but the variability is significant). Statistical uncertainties in the trapped and interplanetary ACR intensities are shown in the figures. Systematic errors due to our method of data analysis are difficult to quantify and are not shown. Implications of these results for trapped particle lifetimes and loss mechanisms are discussed below.

Pitch angle distribution

The function $V(\alpha_1)$ that contains the pitch angle dependence of the trapped ACR oxygen intensity is shown with 5° resolution and normalized at 90° in Figure 3. This represents an average over the entire time period of Figure 1 weighted by the number of counts recorded at each time. Subsets of the data show that the pitch angle distribution has not varied significantly from the average shown in the figure, although the angular resolution of the measurements has decreased from ~1° to several degrees during the SAMPEX mission.

The number of counts in each pitch angle bin is shown in the lower part of Figure 3. The dip at 90° is a result of the relatively short observing time at these pitch angles. The number of counts also represents a weighting function for the average over pitch angles of the intensity shown in Figure 1. It maximizes at ~68° and ~112°.

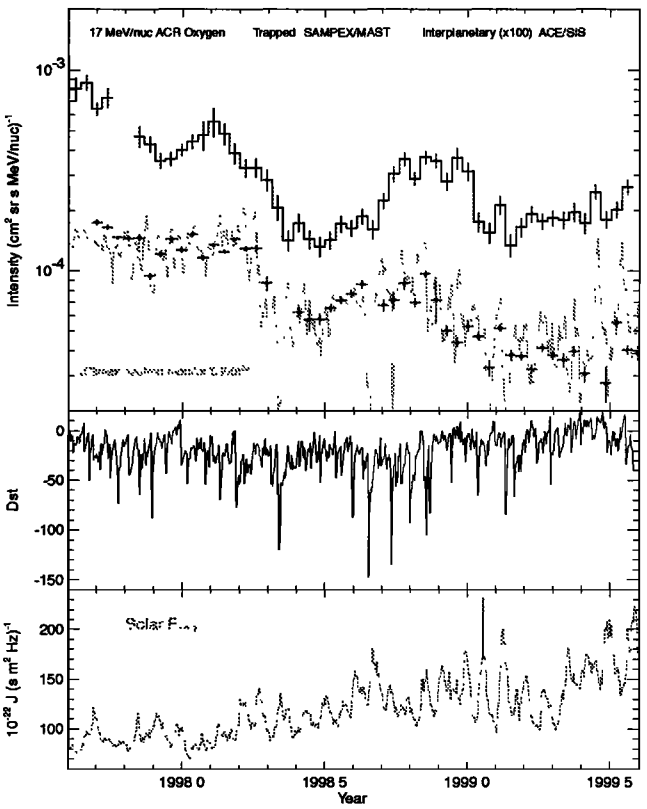

Figure 2. Recent trapped ACR intensity versus time with 13.5-day averages. Also shown are the interplanetary ACR intensity, daily averaged scaled neutron monitor rate, daily averaged geomagnetic D_{st} index, and daily averaged solar 10.7 cm radio flux.

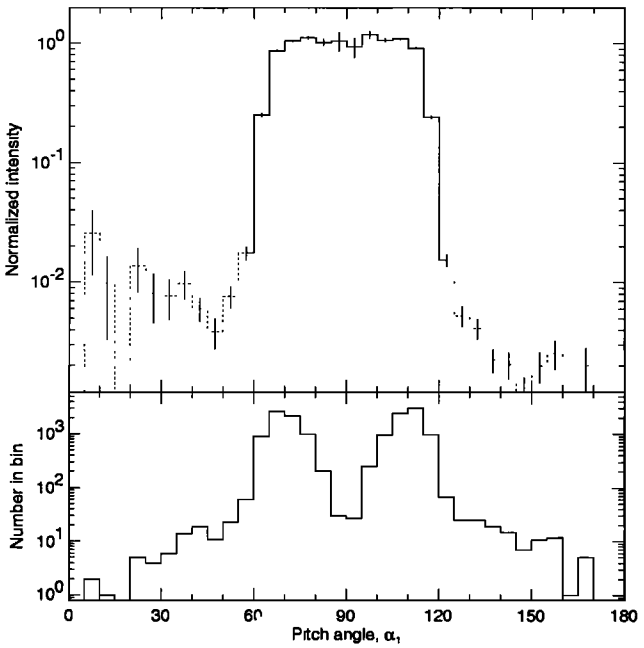

Figure 3. Trapped ACR oxygen pitch angle distribution normalized to the value at $\alpha_1 = 90°$ and number per 5° bin from the entire time interval. Loss cone data (dashed line) are not included in the intensity calculations.

The results in Figure 3 are consistent with an intensity that is nearly independent of pitch angle outside the atmospheric loss cones at ~60° and ~120°, and a factor of at least ~100 lower in the loss cones (the loss cones are not included in the intensity calculations). The observation of a flat pitch angle distribution between the loss cones is different from earlier preliminary estimates [*Selesnick et al.*, 1997] that showed a dip near 90°. We have found that the earlier estimates of the pitch angle distribution were in error due to an excessive round-off in the L shell value used to compile the livetime for each pitch angle bin. The error has now been corrected.

Energy spectra

The function $U(E, L)$ that contains the energy and L dependencies of the trapped ACR oxygen intensity is shown in Figure 4. It is normalized by the maximum intensity, observed at $L = 2$ and $E = 17$ MeV/nucleon. The energy spectra are averaged over 2° in invariant latitude centered at the indicated L values. The bins are logarithmically spaced in energy above 16 MeV/nucleon. The results are consistent with earlier estimates [*Selesnick et al.*, 1995a, 1997] and have better statistical accuracy. They also represent a time average over the interval of Figure 1.

Discussion

Trapped particle losses in the outer radiation belt ($L \sim$ 3 to 5) are often associated with geomagnetic activity. This is less true for losses of inner radiation belt particles ($L \sim$ 1 to 2.5) and the losses of the trapped ACR are not well correlated with the D_{st} geomagnetic index (Figure 2). Another possible loss mechanism is atmospheric energy degradation. The flat pitch angle distribution (Figure 3) is consistent with a balance between source and loss rates

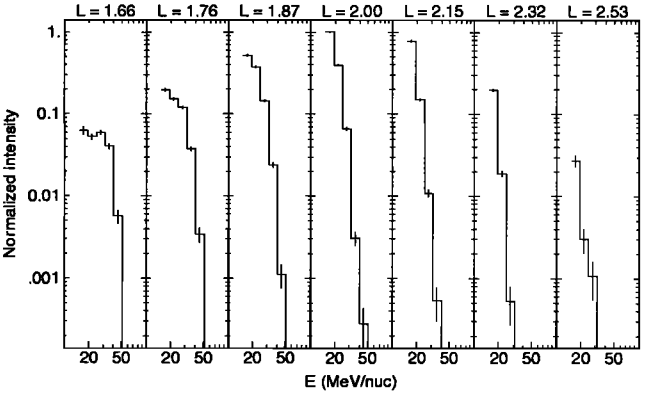

Figure 4. Energy spectra of trapped ACR oxygen at the indicated L values averaged over the entire time interval and normalized to the intensity at 17 MeV/nucleon and $L = 2$.

both of which are proportional to the atmospheric density [*Selesnick et al.*, 1995a]. This would be true if a single atomic interaction in the atmosphere is sufficient to strip enough electrons to trap the interplanetary ACR and if atmospheric energy degradation is the principal trapped ACR loss mechanism. The loss rate must also be fast enough to allow the trapped ACR intensity to change in response to the source as shown in the results described above. Lifetimes of trapped particles based on energy loss in a drift averaged model atmosphere were calculated by *Selesnick and Mewaldt* [1996]. The results for $L = 2.1$ and three values of $F_{10.7}$, which parameterizes the solar cycle dependence of the upper atmospheric densities, are shown in Figure 5 as a function of α_1 and of the equatorial pitch angle α_0. They are most relevant to the SAMPEX observations near $\alpha_1 = 68°$ ($\alpha_0 = 22°$) where the data collection rate maximizes. In this

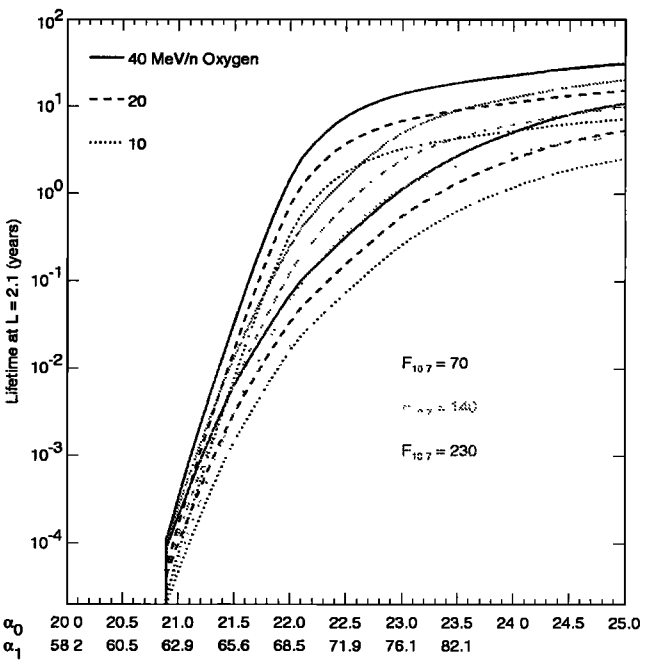

Figure 5. Trapped oxygen lifetimes calculated from a drift averaged model atmosphere at three values of $F_{10.7}$ and three kinetic energies.

case the lifetimes of 20 MeV/nucleon oxygen vary from a few months at solar minimum conditions ($F_{10.7} = 70$) to a few days at solar maximum conditions ($F_{10.7} = 230$). During the period of decreasing ACR intensity the intermediate value of $F_{10.7} = 140$ may be most appropriate (Figure 1) and the corresponding lifetime is ~1 month. The decreasing lifetime with increasing $F_{10.7}$ may account for the apparently more rapid trapped ACR time variations toward the end of the interval shown in Figure 2 which correspond to similar variations in the interplanetary ACR and neutron monitor rate. At altitudes well above those observable by SAMPEX the lifetimes become comparable to the 11-year solar cycle even at solar maximum conditions, so that the trapped ACR may be less variable at those altitudes.

The energy spectra results (Figure 4) are consistent with the theory of ACR trapping at energies above the geomagnetic cutoff and subsequent energy degradation in the atmosphere [*Blake and Friesen*, 1976; *Tylka*, 1994; *Selesnick et al.*, 1995a]. This produces the observed soft spectrum at high energies and high L shells and the hard spectrum at low energies and low L shells. The spectrum above the cutoff energy is softer than the interplanetary ACR spectrum and this was previously ascribed to an hypothesized energy dependence in the trapping efficiency [*Selesnick et al.*, 1995a]. More recent measurements of ACR charge states [*Mewaldt et al.*, 1996] show that the trapped ACR spectrum above the cutoff energy is similar to the soft energy spectrum of singly ionized interplanetary ACR, the harder (>25 MeV/nucleon) interplanetary ACR being predominantly multiply ionized. This may indicate that only the singly ionized ACR are efficiently trapped.

Acknowledgments. This work was supported by NASA Cooperative Agreement 26979B with the Aerospace Corporation and by NASA grant NAS5-2963. The Climax neutron monitor is supported by National Science Foundation Grant ATM-9613963.

References

Blake, J. B. and L. M. Friesen, A technique to determine the charge state of anomalous low energy cosmic rays, it Proc. 15th International Cosmic Ray Conference, 7, 30, 1976.

Cook, W. R., et al., A mass spectrometer telescope for studies of the isotopic composition of solar, anomalous and galactic cosmic ray nuclei, *IEEE Trans. Geoscience Remote Sensing, 31*, 557–, 1993.

Cummings, J. R., et al., New evidence for geomagnetically trapped anomalous cosmic rays, *Geophys. Res. Lett., 20*, 2003–2006, 1993.

Grigorov, N. L., et al., Evidence for anomalous cosmic ray oxygen ions in the inner magnetosphere, *Geophys. Res. Lett., 18*, 1959–1962, 1991.

Looper, M. D., et al., Trapped anomalous cosmic rays near the geomagnetic cutoff, *J. Geophys. Res., 101*, 24,747–24,753,1996.

Mazur, J. E., et al., Argon and other elements in the 1-4 MeV/nucleon trapped anomalous cosmic ray population, *Geophys. Res. Lett.*, in press?, 1999.

Mewaldt, R. A., et al., The return of the anomalous cosmic rays to 1 AU in 1992, *Geophys. Res. Lett., 20*, 2263–2266, 1993.

Mewaldt, R. A., et al., Evidence for multiply charged anomalous cosmic rays, *Astrophys. J. (Letters), 466*, L43–L46, 1996.

Miyasaka, H., et al., Observation of trapped anomalous cosmic rays with MIDORI satellite, *Proc. 26th International Cosmic Ray Conference, 2*, 1999.

Selesnick, R. S. et al., Geomagnetically trapped anomalous cosmic rays, *J. Geophys. Res., 100*, 9503–9518, 1995a.

Selesnick, R. S. et al., Observations of geomagnetically trapped anomalous cosmic rays, *Proc. 24th International Cosmic Ray Conference, 4*, 1013–1016, 1995b.

Selesnick, R. S., et al., Geomagnetically trapped anomalous cosmic rays at solar minimum, *Proc. 25th International Cosmic Ray Conference, 2*, 305–308, 1997.

Selesnick, R. S. and R. A. Mewaldt, Atmospheric production of radiation belt light isotopes, *J. Geophys. Res., 101*, 19,745–19757, 1996.

A. J. Tylka, Theoretical modeling and interpretation of trapped anomalous cosmic rays, *Proc. 23rd International Cosmic Ray Conference, Invited, Rapporteur and Highlight Papers*, p. 465, 1994.

R. S. Selesnick, The Aerospace Corporation, P.O. Box 92957-M2/259, Los Angeles, CA 90009-2957 (e-mail: richard.s.selesnick@aero.org)

A. C. Cummings, R. A. Leske, R. A. Mewaldt, E. C. Stone, California Institute of Technology, Pasadena, CA 91125

J. R. Cummings, Washington University, St. Louis, MO 63130

(Received March 1, 2000; accepted April 13,2000.)